RESEARCH ARTICLE

POLYMERS

A synthetic polymer system with repeatable chemical recyclability

Jian-Bo Zhu, Eli M. Watson, Jing Tang, Eugene Y.-X. Chen*

The development of chemically recyclable polymers offers a solution to the end-of-use issue of polymeric materials and provides a closed-loop approach toward a circular materials economy. However, polymers that can be easily and selectively depolymerized back to monomers typically require low-temperature polymerization methods and also lack physical properties and mechanical strengths required for practical uses. We introduce a polymer system based on γ-butyrolactone (GBL) with a trans-ring fusion at the α and β positions. Such trans-ring fusion renders the commonly considered as nonpolymerizable GBL ring readily polymerizable at room temperature under solvent-free conditions to yield a high–molecular weight polymer. The polymer has enhanced thermostability and can be repeatedly and quantitatively recycled back to its monomer by thermolysis or chemolysis. Mixing of the two enantiomers of the polymer generates a highly crystalline supramolecular stereocomplex.

Various approaches (*1*–*5*) have been pursued to address the unsustainable annual generation and disposal of several hundred million metric tons of synthetic polymers, with the goal of a circular plastics economy (*6*). The use of renewable resources as feedstock materials (*7*, *8*) generally does not address materials' end-of-use problems. The development of biodegradable polymers (*9*) for biological recycling (*10*) also provides a partial solution but fails to recover valuable building block chemicals. Degraded materials, especially those that only partially degrade, can also cause unintended environmental consequences. Mechanical reprocessing (*11*) tends to degrade the quality of the polymers. In contrast, chemical recycling (*12*, *13*) can allow for recovery of the precursor building block chemicals via depolymerization or creative reuse or repurposing through the generation of value-added materials (*14*–*16*). With specifically designed monomers, reaction conditions can be used to select the direction of the monomer-polymer equilibrium or the closed-loop chemical cycle, with low temperatures and bulk or high monomer concentrations favoring polymerization and high temperatures or dilution triggering depolymerization. Several classes of recently designed recyclable polymers operate under this thermodynamic principle, such as poly[2-(2-hydroxyethoxybenzoate)] (*17*, *18*), poly(β-methyl-δ-valerolactone) (*19*), and a polycarbonate (PC) derived from copolymerization of CO_2 with a *meso*-epoxide (*20*). Poly[2-(2-hydroxyethoxybenzoate)] exhibited relatively low glass (~27°C), melting (~69°C), and decomposition (~146°C) temperatures; the thermostability of the PC was also limited (below 260°C), and its depolymerization underwent decarboxylation.

However, the chemical recycling approach still faces challenges, including the selectivity involved in chemical recycling processes and circular monomer-polymer-monomer cycles, as well as trade-offs between polymers' depolymerizability and properties. A notable example for depolymerization selectivity is biodegradable poly(L-lactide) [P(L-LA)], which produces a mixture of many products upon thermolysis (*21*) or a mixture of LA stereoisomers and cyclic oligomers upon chemolysis with an Sn catalyst (*22*), thus requiring substantial separation and purification before the recovered L-LA can be reused. Polymers with a low ceiling temperature (T_c) (*23*, *24*) are readily depolymerizable under mild conditions, but they typically do not have robust enough physical and mechanical properties to be useful for most common applications. For example, poly(γ-butyrolactone) (PGBL), synthesized via catalyzed ring-opening polymerization (ROP) of the renewable, nonstrained, thermodynamically highly stable five-membered γ-butyrolactone (GBL) (*25*, *26*), can be selectively and quantitatively depolymerized back to GBL upon heating of the bulk material at 260° or 300°C, depending on PGBL topology (*27*, *28*). However, the synthesis of PGBL requires energy-intensive, industrially undesirable low-temperature conditions (typically –40°C), and PGBL exhibits limited thermostability and crystallinity, with a low melting transition temperature (T_m) of ~60°C. Another example of a completely recyclable polymer was produced through the chemoselective ROP of bioderived α-methylene-γ-butyrolactone; however, not only was a low temperature (–60°C) required for the polymer synthesis, but the resulting polymer was also a noncrystalline amorphous material (*29*).

Department of Chemistry, Colorado State University, Fort Collins, CO 80523-1872, USA.
*Corresponding author. Email: eugene.chen@colostate.edu

Room temperature, solvent-free polymerization to high–molecular weight polymers

To design monomer and polymer structures that can deliver desired properties, it is advantageous to keep the highly stable, five-membered GBL core so that the complete chemical recyclability of the designed polymers can be preserved (for both thermodynamic and kinetic reasons). We reasoned that the ring strain of the parent (nonstrained five-membered GBL), or the thermodynamic polymerizability, can be tuned via suitable substituents and substitution patterns on the GBL ring. *trans*-Hexahydro-2(3*H*)-benzofuranone [i.e., 4,5-*trans* six-membered ring–fused GBL (4,5-T6GBL)] was found to be polymerizable even at 40°C by typical anionic initiators but not by a coordination polymerization catalyst such as tin(II) octoate, whereas the cis-fused isomer is completely inert toward ROP (*30*). However, the resulting product was reported to be only an oligomer, with a number-average molecular weight (M_n) up to only 6.2 kg/mol [by gel permeation chromatography (GPC)] or 2.6 kg/mol [by nuclear magnetic resonance (NMR)]. We hypothesized that removing the substituent at the 5 (or γ) position of the GBL ring could not only further enhance the thermodynamic polymerizability (by increasing the ring strain) and rate of polymerization (by releasing the steric pressure at the ester $-OC_\alpha H$), thus affording useful high–molecular weight polymers in short time periods, but also render polymers with possibly high crystallinity assisted by ordered secondary structures and/or $OC_\alpha H$–O=C hydrogen bonds (*31*–*33*) between polyester chains. Guided by these hypotheses, we arrived at 3,4-T6GBL (**M1**), where the cyclohexyl ring is trans-fused to GBL at the α and β positions and the γ position is left unsubstituted to enhance polymerizability, reaction rates, and H bonding. This monomer can be prepared on relatively large scales from commercially available *trans*-1,2-cyclohexanecarboxylic acid anhydride (*34*).

The polymerizability of **M1** was probed via measuring the thermodynamics of its ROP with a discrete molecular catalyst, yttrium complex **Y1** (*35*) (Fig. 1A), which is known to be effective for the ROP of the parent GBL (*27*), revealing standard-state thermodynamic parameters of ΔH°_p (change in enthalpy of polymerization) = –20 kJ mol^{-1} and ΔS°_p (change in entropy of polymerization) = –72 J mol^{-1} K^{-1} (figs. S9 and S10). The T_c was calculated to be 0°, 62°, or 88°C for an initial **M1** concentration ($[\mathbf{M1}]_0$) of 1.0, 5.0, or 8.2 (bulk) M, respectively. These data showed that **M1** exhibits much higher thermodynamic polymerizability than GBL, as indicated by a much larger negative change in enthalpy and a substantially elevated T_c: ΔH°_p = –20 kJ mol^{-1} versus –5.4 kJ mol^{-1} and T_c = 0°C (1.0 M) versus –136°C (1.0 M) for the ROP of **M1** and GBL, respectively. Accordingly, we chose the solvent-free, bulk condition to perform the polymerization at room temperature, as summarized in table S1. Quantitative conversion of **M1** was achieved even with common anionic initiators such as potassium *tert*-butoxide and TBD (1,5,7-triazabicyclo[4.4.0]dec-5-ene), but

the product was not that of a polymer; instead, **M1** was isomerized under the basic conditions to its cis isomer, which is nonpolymerizable, as verified by its independent synthesis and subsequent polymerization surveys with different catalysts and conditions (table S2). To overcome this isomerization issue, we used a coordinative-insertion ROP catalyst, La[N($SiMe_3$)$_2$]$_3$ (where Me is methyl) (**La1**), as La is more earth abundant and less expensive within the lanthanide series (*36*) and was demonstrated to be effective for the ROP of GBL (*27*). **La1** exhibited high selectivity and activity toward the ROP to afford poly-**M1** [P(**M1**)], achieving greater than 80% conversion with 0.2 or 0.1 mole % (mol %) catalyst loading. For example, with a monomer (M)/catalyst (cat)/initiator (I) ratio of [**M1**]/[**La1**]/[Ph_2CHCH_2OH] (where Ph is phenyl) = 500/1/3, the ROP occurred rapidly to reach 73% **M1** conversion in under 1 min. At 82% conversion, the isolated P(**M1**) was measured by a GPC instrument equipped with multi (18)–angle light scattering and differential refractive index detectors to have a medium M_n of 21.0 kg/mol and an extremely low dispersity index ($Đ$) value of 1.01; this measured M_n is close to the calculated M_n of 19.4 kg/mol, thus indicating a high initiation efficiency of 92%. Lowering the catalyst loading to 0.1 mol % (1000/1/3 ratio) still achieved a relatively high conversion of 84%, producing P(**M1**) with M_n = 46.0 kg/mol and $Đ$ = 1.01. To further increase the molecular weight of the resulting P(**M1**), the M/cat/I ratio was increased to 5000/1/3 with a catalyst loading of 0.02 mol %, affording P(**M1**) a further enhanced M_n (67.9 kg/mol) and a still low $Đ$ (1.01) at 45% conversion. The absolute molecular weight measured by GPC (M_n = 21.0 kg/mol, $Đ$ = 1.01) (table S1, run 2) was close to both the M_n of 19.4 kg/mol calculated on the basis of the [**M1**]/[I] ratio (table S1) and the M_n of 19.9 kg/mol calculated on the basis of the chain ends of the polymer characterized by NMR (figs. S11 and S12), the latter of which also revealed a linear structure {linear P(**M1**) [*l*-P(**M1**)]} and showed high end-group fidelity. The linear structure of the P(**M1**) produced by **La1** with ROH (where R is Ph_2CHCH_2O) was further confirmed by matrix-assisted laser desorption/ionization–time-of-flight mass spectroscopy (MALDI-TOF MS) of a low–molecular weight sample. Specifically, the MS spectrum (fig. S13) consisted of only one series of molecular ion peaks, with the spacing between the two neighboring molecular ion peaks corresponding to the exact molar mass of the repeat unit, **M1** [mass/charge ratio (m/z) = 140.18], as shown by the slope (140.14) of the linear plot of m/z values (y axis) versus the number of **M1** repeat units (x axis). The intercept of the plot, 221.8, represents the total mass of chain ends plus the mass of Na^+ [M_{end} = 198.3 (Ph_2CHCH_2O/H) g/mol + 23.0 (Na^+) g/mol], corresponding to linear structure Ph_2CHCH_2O–[**M1**]$_n$–H.

With the demonstrated ability of **La1** to form PGBL with a cyclic structure when no initiating ROH is added (*27*), we explored the possibility of producing cyclic polymer *c*-P(**M1**) by using **La1** alone. The polymerizations with different catalyst loadings (1.0 to 0.05 mol % **La1**) were rapid and achieved relatively high monomer conversions, from 79 to 84%. Unlike the controlled polymerization with **La1** and 3ROH, where the [**M1**]/[**La1**] ratio could determine the M_n while maintaining a low $Đ$ value of 1.01 for all the *l*-P(**M1**) materials produced (table S1), the polymerizations with **La1** alone afforded polymers with similar M_n values in a narrow range of 73.0 to 85.5 kg/mol coupled with higher $Đ$ values from 1.34 to 1.48, despite a 20-fold change in the [**M1**]/[**La1**] ratio and a 7-fold change in the reaction scale (table S1). These observations indicated that possible cyclization reactions occurred under the neat and room temperature conditions used once a certain chain length was reached, which would create a cyclic polymer structure, *c*-P(**M1**). Consistent with this proposed scenario, no end groups were detected from the NMR spectra of the polymers produced by using **La1** alone (figs. S14 to S16). Analysis of a low–molecular weight sample by MALDI-TOF MS (fig. S17) also revealed no end groups (the linear plot of m/z values versus the number of **M1** repeat units gave an intercept of 23, corresponding to the mass of Na^+). The cyclic structure of *c*-P(**M1**) was further confirmed by GPC analysis with triple detection by a light-scattering detector, a refractometer, and a viscometer. A double-logarithm (Mark-Houwink-Sakurada) plot of intrinsic viscosity [η] versus absolute weight-average molecular weight (M_w) in the lower molecular weight regime (Fig. 1B) showed a lower intrinsic viscosity for *c*-P(**M1**), due to a smaller hydrodynamic volume, than for *l*-P(**M1**). The $[\eta]_{cyclic}/[\eta]_{linear}$ ratio was found to be 0.7, which is in agreement with the theoretically predicted value for this ratio and the experimentally observed value for other cyclic polymers (*37*). Expanding to an optically active cyclic polymer structure, we synthesized two chiral polymers with similar M_w values from the ROP of (*R*)-**M1** with

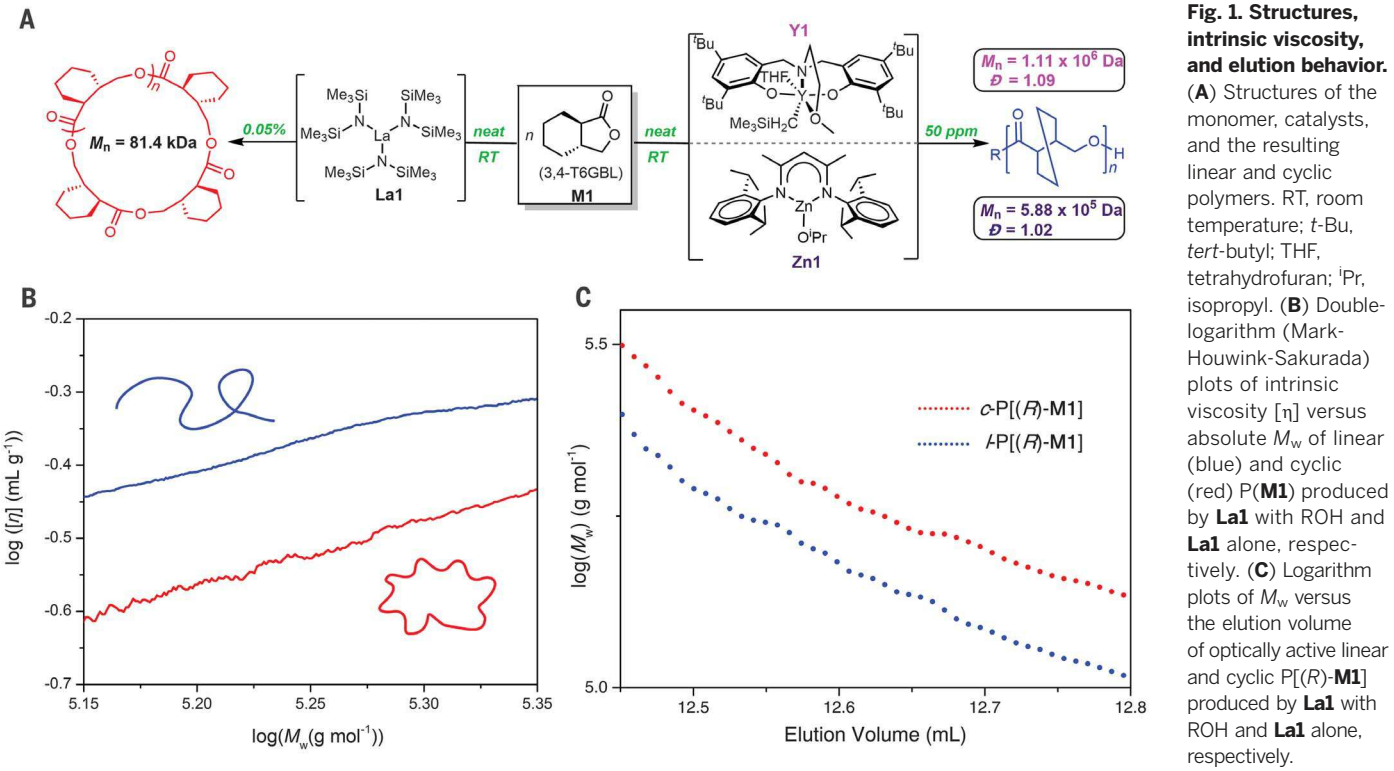

Fig. 1. Structures, intrinsic viscosity, and elution behavior. (**A**) Structures of the monomer, catalysts, and the resulting linear and cyclic polymers. RT, room temperature; *t*-Bu, *tert*-butyl; THF, tetrahydrofuran; ^{i}Pr, isopropyl. (**B**) Double-logarithm (Mark-Houwink-Sakurada) plots of intrinsic viscosity [η] versus absolute M_w of linear (blue) and cyclic (red) P(**M1**) produced by **La1** with ROH and **La1** alone, respectively. (**C**) Logarithm plots of M_w versus the elution volume of optically active linear and cyclic P[(*R*)-**M1**] produced by **La1** with ROH and **La1** alone, respectively.

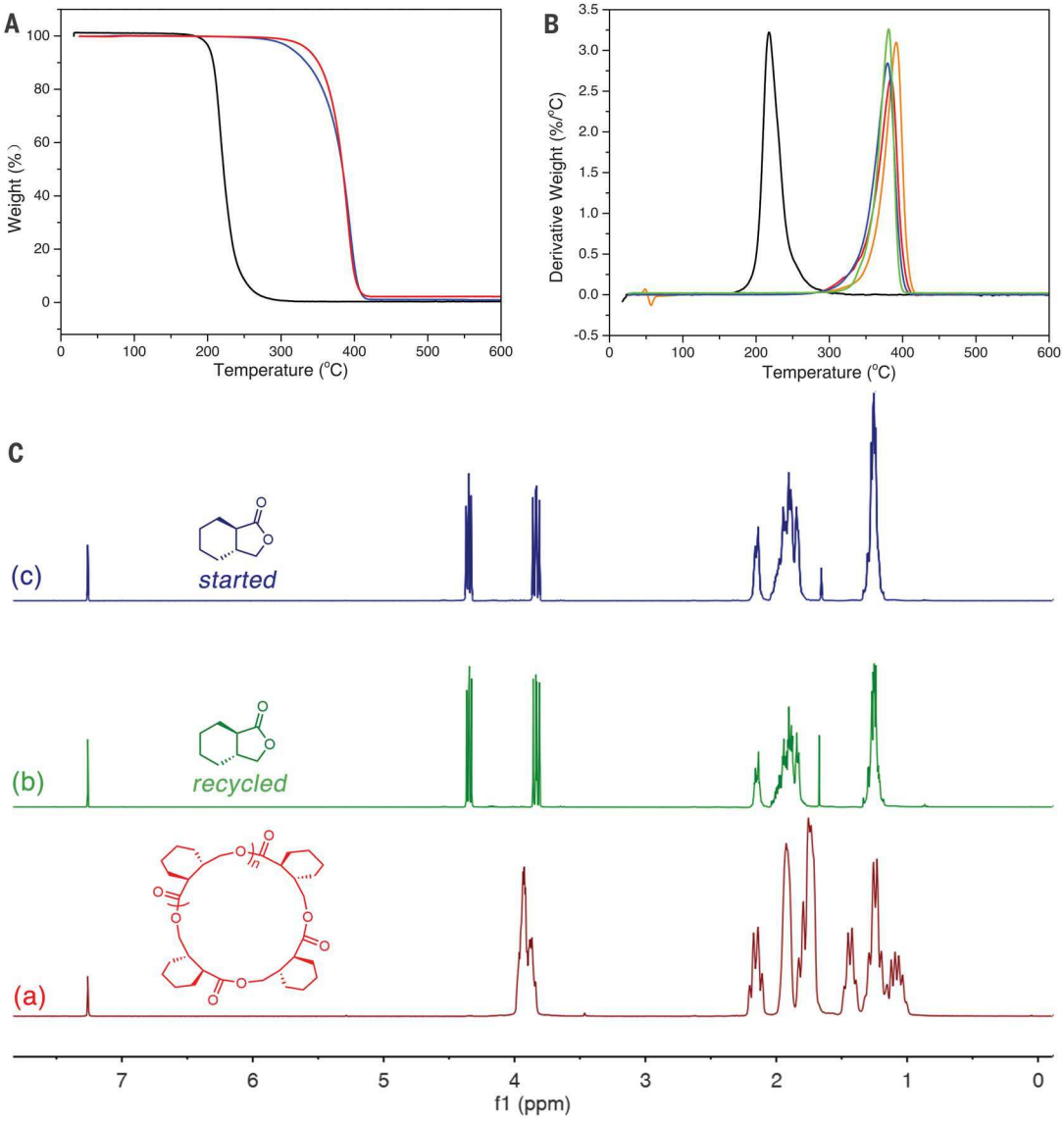

Fig. 2. Thermostability and chemical recyclability of P(M1). (**A**) TGA curves for *c*-P(**M1**) obtained with [**M1**]/[**La1**] = 2000/1 (red) and *l*-P(**M1**) obtained with [**M1**]/[**La1**]/[Ph_2CHCH_2OH] = 500/1/3 (blue) and a comparative example for the linear PGBL obtained with [GBL]/[**La1**]/[Ph_2CHCH_2OH] = 400/1/3 (black). (**B**) Overlays of DTG curves for *l*-P(**M1**) obtained with **Y1** (orange), P[(*R*)-**M1**] with **Y1** (blue), P[(*S*)-**M1**] with **Y1** (red), and a 1:1 P[(*R*)-**M1**]–P[(*S*)-**M1**] blend (green) and a comparative example for linear PGBL (black). (**C**) Overlays of ^{1}H NMR spectra (25°C, $CDCl_3$, with residual solvent peaks at 7.26 and 1.56 ppm for $CHCl_3$ and H_2O, respectively): (a) *c*-P(**M1**); (b) the colorless liquid product recovered after depolymerization (toluene, 2 mol % $ZnCl_2$, 120°C, 24 hours); (c) clean-starting **M1** for comparison.

La1 and ROH and with **La1** alone. The logarithm plots of M_w versus the elution volume revealed that the chiral polymer P[(*R*)-**M1**] obtained in the absence of ROH was eluted later than the polymer obtained in the presence of ROH (Fig. 1C). By analogy to achiral P(**M1**), it can be likewise assigned to a cyclic structure because its hydrodynamic volume is smaller than that of its linear analog.

The synthesis of pure cyclic polymers with appreciable (medium to high) molecular weights, which are critical for polymer topology–property relationship studies, still presents a challenge for many types of polymers. This problem has led to substantial interest in developing synthetic methodologies for cyclic polymers (*38*, *39*), such as the ring-opening metathesis polymerization route to cyclic polyethylene (*40*) and the *N*-heterocyclic carbene–mediated zwitterionic polymerization route to cyclic polylactide (*41*) and poly(α-peptoid)s (*42*). The cleaner formation of *c*-P(**M1**) than of cyclic PGBL (*27*), as demonstrated by the NMR, MS spectra, and $[\eta]_{cyclic}/[\eta]_{linear}$ ratio, is noteworthy.

As the molecular weight of the cyclic polymer is limited by the propensity to cyclize once a certain chain length is reached during the polymerization, we explored other catalyst-initiator systems that could further increase the molecular weight of *l*-P(**M1**). In this context, we arrived at discrete yttrium complex **Y1** supported by the tetradentate amino-bisphenolate ligand bearing a pendant ether group, which has been shown to be highly efficient in the ROP of lactide and lactones (*43*, *44*). With **Y1** as the catalyst and catalyst loading as low as 50 parts per million (ppm), we achieved relatively high **M1** conversions of 80 to 91% (table S1). Thus, in a 10-g polymerization, a high–molecular weight P(**M1**) with $M_n = 1.11 \times 10^6$ g/mol ($Đ = 1.09$) was readily produced under neat and room temperature conditions with only 50 ppm **Y1**. Furthermore, the molecular weight of the resulting polymer could be readily controlled by the addition of the ROH (Ph_2CHCH_2OH) initiator; thus, with the [**M1**]/[**Y1**] ratio of 10000/1 held constant, the equivalent of ROH added (relative to **Y1**) was varied from 25 to 50 to 100, affording *l*-P(**M1**) with correspondingly reduced M_n values from 49.2 kg/mol ($Đ = 1.01$) to 18.4 kg/mol ($Đ = 1.01$) to 11.6 kg/mol ($Đ = 1.01$) (table S1). These M_n values were close to the M_n values calculated on the basis of the [**M1**]/[ROH] ratio and **M1** conversion data, thus demonstrating a high initiation efficiency of >96%. Overall, **Y1** brings about "immortal" ROP (*45*, *46*) of **M1** in the presence of ROH, producing well-defined *l*-P(**M1**) materials with near ideal dispersity (1.01) in a catalytic fashion (affording up to 100 polymer chains per **Y1**).

An environmentally more benign and earth-abundant zinc catalyst, 2,6-diisopropylphenyl-substituted β-diiminate zinc isopropoxide complex [(BDI)ZnO^{i}Pr] (**Zn1**) (*47*), was also examined for the ROP of **M1** at room temperature under neat conditions. The results, summarized in table S1, showed that **Zn1** is also highly effective for this polymerization. For example, with catalyst loading of 0.02 mol %, the ROP achieved 82% conversion

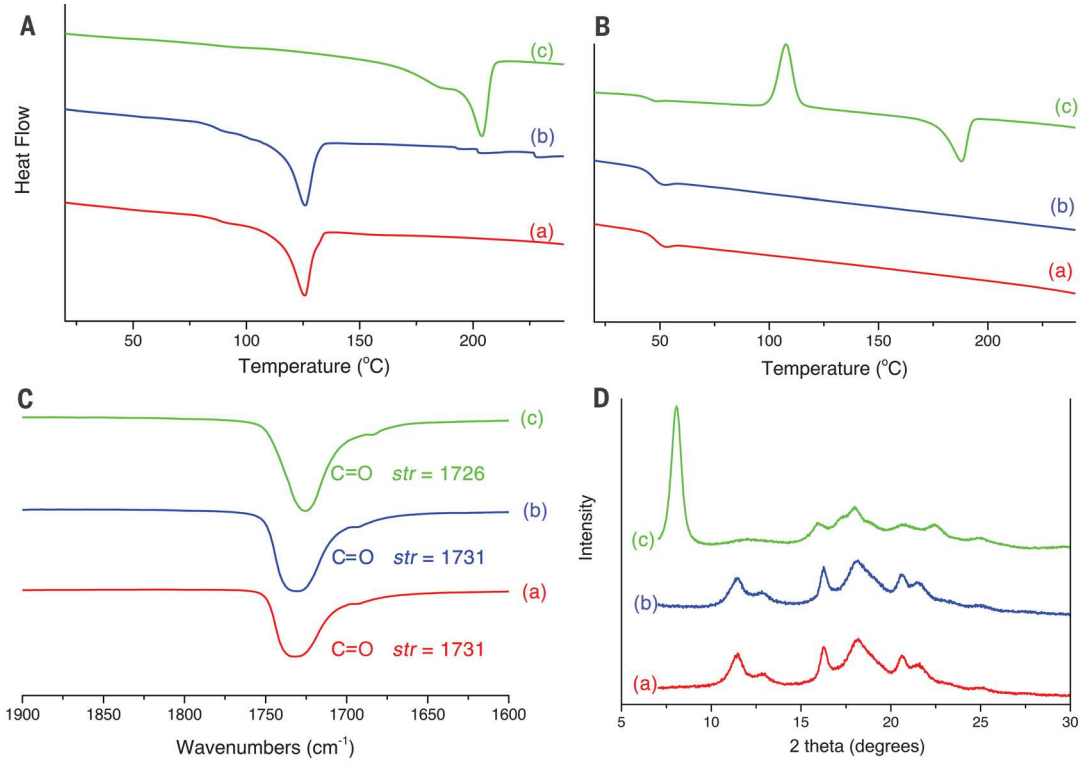

Fig. 3. Thermal transitions and spectroscopic properties. (**A**) DSC first-heating-scan curves (10°C/min). (**B**) DSC second-heating-scan curves [5°C/min for (a) and (b) or 1°C/min for (c), after first cooling at 10°C/min]. (**C**) Overlays of FTIR spectra in the carbonyl stretching region. str, stretching frequency. (**D**) Powder XRD profiles. In all cases, *l*-P(**M1**) polymers were prepared with [**M1**]/[**Y1**] = 1000/1: *l*-P[(*S*)-**M1**] (a, red), *l*-P[(*R*)-**M1**] (b, blue), and 1:1 *l*-P[(*R*)-**M1**]–*l*-P[(*S*)-**M1**] blend or *sc*-P(**M1**) (c, green).

in 3 hours, producing P(**M1**) with a high M_n of 307 kg/mol and an extremely narrow $Đ$ of 1.01. Comparing these data with those obtained with **Y1**—12 hours, 87% conversion, M_n = 363 kg/mol, and $Đ$ = 1.15—under the same conditions shows that, under this set of conditions (room temperature, neat conditions, 0.02 mol % catalyst), the Zn catalyst performed better than the Y catalyst in terms of its higher polymerization activity and lower polymer dispersity.

Thermostability, chemical recyclability, and circular M1-P(M1)-M1 cycle

The thermostability of both linear and cyclic P(**M1**) materials was examined by thermogravimetric analysis (TGA) in terms of onset decomposition temperature T_d (defined by the temperature of 5% weight loss) and maximum decomposition temperature T_{max} [defined by the peak value in the relative derivative thermogravimetry (DTG)]. Comparing TGA curves of the cyclic and linear polymers revealed that *c*-P(**M1**) produced with **La1** alone had a noticeably higher T_d (337°C) than *l*-P(**M1**) obtained with [**M1**]/[**La1**]/[Ph_2CHCH_2OH] = 500/1/3, with T_d = 316°C (Fig. 2A), although the T_{max} values were similar (390° versus 394°C) (figs. S22 and S23). The T_d and T_{max} of *l*-P(**M1**) were 115° and 176°C higher, respectively, than those of the linear PGBL (obtained with [GBL]/[**La1**]/[Ph_2CHCH_2OH] = 400/1/3), which had a T_d of 201°C and a T_{max} of 218°C. The *l*-P(**M1**) produced by **Y1** ([**M1**]/[**Y1**] = 2000) was even more thermally robust, with a high T_d of 342°C and a T_{max} of 391°C (Fig. 2B). The T_d (344°C) of the physical blend of 1:1 P[(*R*)-**M1**]–P[(*S*)-**M1**] was found to be about 17 to 21°C higher than those of the respective enantiomeric polymers (figs. S25 to S29), whereas the T_{max} values varied only slightly (Fig. 2B).

The chemical recyclability of P(**M1**) materials was examined by both thermolysis at high temperatures and chemolysis in the presence of a catalyst at milder temperatures. An *l*-P(**M1**) sample (M_n = 46.0 kg/mol, $Đ$ = 1.01) prepared with [**M1**]/[**La1**]/[Ph_2CHCH_2OH] = 1000/1/3 was heated in a sealed tube at ≥300°C for 1 hour; gravimetric and NMR analyses (figs. S30 and S31) of the resulting colorless liquid showed that monomer **M1** was recovered in a pure state at a quantitative yield. Likewise, heating a *c*-P(**M1**) sample (M_n = 82.0 kg/mol, $Đ$ = 1.43) prepared with [**M1**]/[**La1**] = 100/1 at ≥300°C for 24 hours also afforded the recycled monomer in a pure state (figs. S32 and S33) at a quantitative yield. To reduce the energy input in the recycling process, the chemical recyclability of P(**M1**) was also investigated by chemolysis with a catalytic amount of a simple metal salt ($ZnCl_2$) at 120°C. Thus, subjecting either *l*-P(**M1**) (figs. S34 and S35) or *c*-P(**M1**) (Fig. 2C and figs. S36 and S37) to the above-listed mild chemolysis conditions also demonstrated the full chemical recyclability.

The circular monomer-polymer-monomer cycle was examined through three consecutive polymerization-depolymerization cycles on a multigram scale. Thus, pure **M1** was first polymerized by **Zn1** to well-defined P(**M1**) ($Đ$ = 1.01) after achieving 85% conversion, which is the typical conversion achieved under the ambient temperature and neat conditions used (the unreacted monomer can be recovered). The isolated and purified P(**M1**) was then subjected to chemolysis in the presence of a simple metal salt ($ZnCl_2$, 2 mol %) at 180°C under vacuum pressure (0.01 torr); the collected colorless liquid was confirmed to be pure **M1** by ^{1}H NMR analysis (figs. S38 to S44). The recovered monomer (97% isolated yield) was repolymerized directly without further purification by **Zn1** to produce well-defined P(**M1**) ($Đ$ = 1.02), achieving the same conversion (85%). This process was repeated three times, and the mass balance of the regenerated polymer product and the recovered monomer was tracked over the three consecutive polymerization-depolymerization cycles, showing essentially quantitative recovery of pure **M1** (96 to 97% isolated yield) after each cycle. This recovered **M1** can be directly repolymerized without a decrease in the subsequent monomer conversion and polymer quality.

Physical blending to yield highly crystalline stereocomplexed material

Physical blending of enantiomers of certain chiral polyesters in a stoichiometric ratio offers a powerful strategy to generate crystalline stereocomplexed (*sc*) materials that often exhibit much enhanced materials properties, such as increased T_m and crystallization rate, compared with their constituent enantiomers (*48*–*52*). In this context, a 1:1 physical blend of enantiomeric isotactic polymers (table S3 and figs. S48 to S53) derived from enantiomeric monomers, either linear enantiomers *l*-P[(*R*)-**M1**] and *l*-P[(*S*)-**M1**] produced with [**M1**]/[**Y1**] = 1000/1 or cyclic enantiomers *c*-P[(*R*)-**M1**] and *c*-P[(*S*)-**M1**] produced with [**M1**]/[**La1**] = 500/1, showed substantially different thermal properties and solubility as well

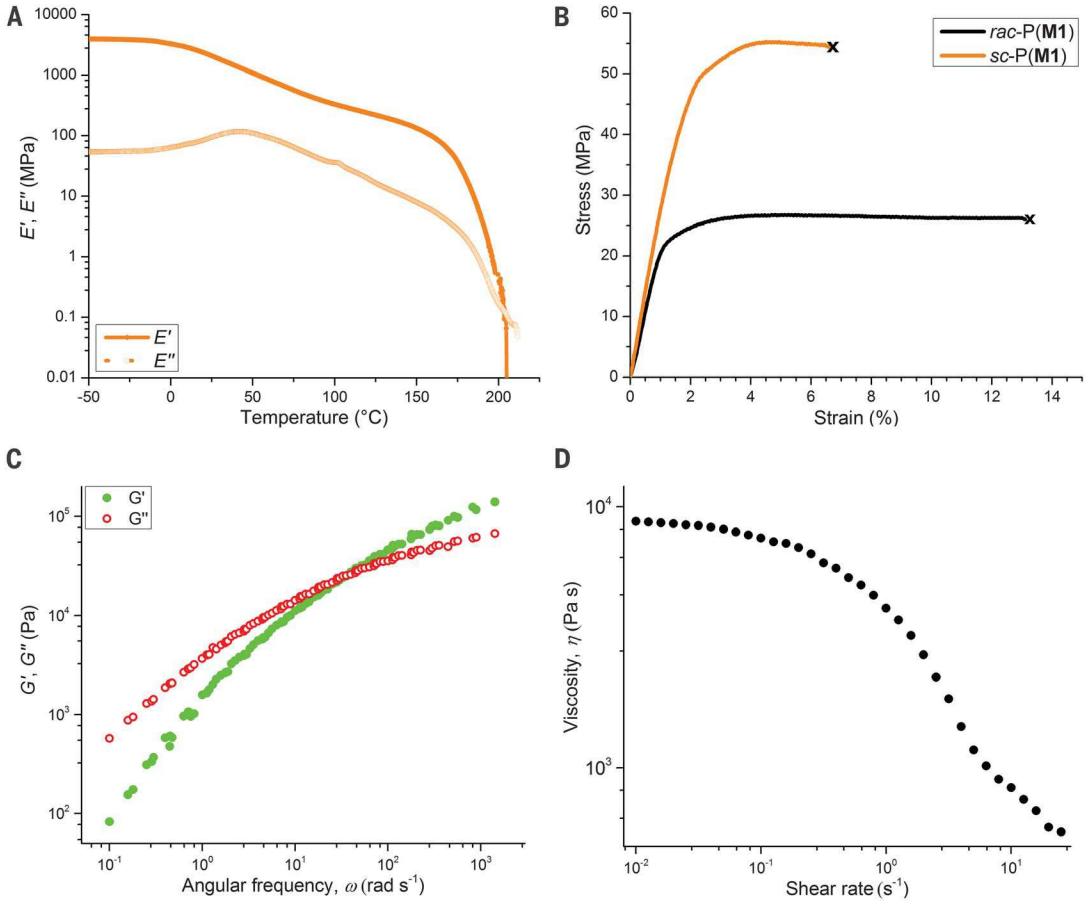

Fig. 4. Mechanical and rheological properties. (**A**) Overlay of storage modulus E' and loss modulus E'' for *sc*-P(**M1**) measured by DMA (tension film mode, 0.05% strain, 1 Hz, 3°C min^{-1}). (**B**) Stress-strain curves for *rac*-P(**M1**) and *sc*-P(**M1**) measured by tensile testing (5.0 mm/min, room temperature, with the break point indicated by ×). (**C**) Rheology master curve (dynamic storage modulus G' and loss modulus G'' versus angular frequency ω) for *rac*-P(**M1**), reported as a time-temperature superposition curve at reference temperature 215°C. (**D**) Dynamic shear viscosity of *rac*-P(**M1**) as a function of the shear rate measured at 215°C.

as noticeably different spectroscopic features from the parent enantiomers. Differential scanning calorimetry (DSC) curves for the first heating scans (Fig. 3A) of the linear enantiomeric polymers, previously crystallized from $CHCl_3$, displayed a crystalline peak with T_m = 126°C (heat of fusion ΔH_m = 28 to 32 J/g), but the 1:1 blend produced much higher melting and heat of fusion values, with T_m = 203°C and ΔH_m = 53 J/g. More notably, on the second heating scans (after cooling at 10°C/min) only the physical blend continued to show a melting peak of T_m = 188°C (T_c = 108°C), whereas the enantiomeric polymers became amorphous, displaying only a glass transition temperature T_g of ~49°C (Fig. 3B). These results indicate that these enantiomeric polymers have relatively low crystallization rates and that stereocomplexation in the blend markedly enhanced not only the crystallinity but also the crystallization rate. Linear enantiomeric polymers produced by the [**La1**]-3[Ph_2CHCH_2OH] system displayed more or less the same DSC curves on the first and second heating scans (figs. S55 and S56). Furthermore, a comparison of DSC curves for *c*-P(**M1**) showed the same trend: The first heating scans revealed a T_m of 127°C (ΔH_m = 34 to 37 J/g) for the enantiopure polymers but a much higher T_m of 198°C and ΔH_m of 61 J/g for the *c*-P[(*R*)-**M1**]–*c*-P[(*S*)-**M1**] blend (figs. S65 and S66), and the second heating scans showed a melting peak of T_m = 188°C (T_c = 122°C) only for the blend (fig. S66).

Overlays of Fourier transform infrared (FTIR) spectra in the carbonyl stretching region (Fig. 3C and fig. S70) revealed the red shift of the C=O stretching frequency ($\nu_{C=O}$) for the blend of the two linear enantiomeric polymers to a wave number 5 cm^{-1} lower than that for the parent enantiomers. Likewise, a red shift of 7 cm^{-1} was also observed for the blend of the two cyclic enantiomers relative to the parent enantiomers (figs. S71 and S72). These results are consistent with the hypothesis that the blend forms a stereocomplex, *sc*-P(**M1**), assisted by the weak to moderate $OC_\alpha H$–O=C hydrogen bonds. Powder x-ray diffraction (XRD) profiles (Fig. 3D) of enantiomeric *l*-P[(*R*)-**M1**] [(a) in Fig. 3D] and *l*-P[(*S*)-**M1**] (prepared using [**M1**]/[**Y1**] = 1000/1), as well as their 1:1 *l*-P[(*R*)-**M1**]–*l*-P[(*S*)-**M1**] blend or *sc*-P(**M1**), all crystallized from $CHCl_3$, revealed substantially different crystalline diffraction patterns of the blend in comparison with the parent enantiomers. Chiefly, whereas the two enantiomeric polymers showed identical patterns (consisting of four major diffraction signals at 11.5°, 16.2°, 18.2°, and 20.6°, along with three minor peaks at 12.8°, 21.6°, and 25.2°), the blend exhibited a new, intense diffraction peak at 8.1° [*d* spacing (the spacing between adjacent planes) = 1.1 nm] and was also devoid of the two signals (major, 11.5°, and minor, 12.8°) present in the enantiomers, which is attributable to the formation of the stereocomplex. Although P[(*R*)-**M1**] or P[(*S*)-**M1**] is readily soluble in common polar organic solvents such as $CHCl_3$, CH_2Cl_2, and *N*,*N*′-dimethylformamide (DMF), *sc*-P(**M1**) is only partially soluble in $CHCl_3$ and insoluble in CH_2Cl_2, tetrahydrofuran, and DMF. Overall, the above corroborative evidence showed that a nanocrystalline stereocomplex formed between the two enantiomeric P(**M1**) polymers and that such a stereocomplex exhibited markedly enhanced crystallinity, crystallization rate, and solvent resistance over those of the parent enantiomers.

In contrast, mixing of enantiomeric polymers P[(+)-4,5-T6GBL] and P[(−)-4,5-T6GBL] (table S3) in a 1:1 stoichiometric ratio, followed by crystallization, yielded a physical blend exhibiting thermal properties and spectroscopic characteristics essentially identical to those of either the starting enantiomeric polymer or the racemic polymer P[(±)-4,5-T6GBL]. DSC curves (fig. S45) for the two enantiomeric polymers and their physical blend displayed the same features of an amorphous material, with a T_g of ~72°C. FTIR spectra (figs. S46 and S47) also revealed the same absorption features, with an identical $\nu_{C=O}$ stretching frequency of 1725 cm^{-1} observed for all of the three polymers (two enantiomeric polymers and their 1:1 blend). Overall, the above collective

evidence showed that no stereocomplexation occurred upon mixing of these two enantiomeric polymers, and thus no enhancement of properties occurred through blending.

Mechanical and rheological properties

The thermomechanical properties of the amorphous polymer derived from racemic **M1** [*rac*-P(**M1**)] prepared with **Y1** (M_n = 875 kg/mol, $Đ$ = 1.07) (table S1, run 19) and semicrystalline stereocomplex *sc*-P(**M1**) prepared with **Y1** (table S3, runs 4 and 8) were examined by dynamic mechanical analysis (DMA) in a tension film mode. The thermomechanical spectra of *sc*-P(**M1**) (Fig. 4A) and *rac*-P(**M1**) (fig. S83) show that, at room temperature (the glassy state), both *sc*-P(**M1**) and *rac*-P(**M1**) exhibited high storage modulus (E') values, although E' (1.58 ± 0.44 GPa) of *sc*-P(**M1**) was somewhat higher than that (1.47 ± 0.25 GPa) of *rac*-P(**M1**). However, after the glass transition region with similar T_g values [83 to 90°C, as defined by the peak maxima of tan δ, the loss modulus/storage modulus ratio (E''/E')] (fig. S84), E' of *rac*-P(**M1**) dropped by more than three orders of magnitude and then quickly went to the viscous flow state. In contrast, E' of *sc*-P(**M1**) decreased only by approximately one order of magnitude after T_g, and the material still maintained a high E' in the rubbery plateau until reaching a flow temperature of ~180°C, characteristic of a semicrystalline material having a high T_m (186°C by DSC).

Tensile testing of dog-bone–shaped specimens of *rac*-P(**M1**) and *sc*-P(**M1**) yielded stress-strain curves (Fig. 4B), revealing that semicrystalline *sc*-P(**M1**) exhibited a much higher ultimate tensile strength (σ_B = 54.7 ± 4.0 MPa) and Young's modulus (E = 2.72 ± 0.25 GPa) than amorphous *rac*-P(**M1**) (σ_B = 26.2 ± 3.2 MPa, E = 1.85 ± 0.30 GPa). As a glassy material, *sc*-P(**M1**) displayed an elongation at break (ε_B = 6.5 ± 1.2%), and the ε_B value for *rac*-P(**M1**) was approximately doubled, with ε_B = 13.1 ± 3.5%. Overall, the key thermal and mechanical properties of the crystalline P(**M1**) (T_g ~ 50°C, T_m ~ 188°C, T_d ~ 340°C; σ_B ~ 55 MPa, E ~ 2.7 GPa, ε_B ~ 7%) compare well to those of typical crystalline P(L-LA) materials (T_g ~ 54° to 59°C, T_m ~ 159° to 178°C, T_d ~ 235° to 255°C; σ_B ~ 28 to 50 MPa, E ~ 1.2 to 3.0 GPa, ε_B ~ 2 to 6%) (*53*).

The angular frequency (ω) dependencies of the dynamic storage or elastic modulus (G') and loss or viscous modulus (G'') of *rac*-P(**M1**) and *sc*-P(**M1**) were characterized at six different temperatures (165°, 175°, 185°, 195°, 205°, and 215°C) in the linear viscoelastic regime (1.0% strain) established by the strain sweeps at 215°C (figs. S85 and S86). The data obtained from frequency sweep experiments at each temperature were compiled to generate a master curve reported as a time-temperature superposition curve at reference temperature 215°C [Fig. 4C for *rac*-P(**M1**) and fig. S87 for *sc*-P(**M1**)]. A G' and G'' crossover point where G' becomes larger than G'', indicating the transition from the terminal (viscous) to the rubbery (elastic) region, was seen for both *rac*-P(**M1**) and *sc*-P(**M1**). The crossover frequencies measured at 165°, 175°, 185°, 195°, 205°, and 215°C for *rac*-P(**M1**) were found to be 0.43, 0.75, 1.21, 1.95, 3.18, and 4.89 Hz, corresponding to relaxation times of 2.32, 1.33, 0.83, 0.51, 0.31, and 0.21 s, respectively. The crossover frequencies observed for *sc*-P(**M1**) were more than six times higher at each of the same temperatures, thus giving rise to much shorter relaxation times, from 0.34 s (165°C) to 0.03 s (215°C). For the high–molecular weight *rac*-P(**M1**) (M_n = 875 kg/mol), the melt processability was preliminarily tested by examining the dynamic melt viscosity as a function of the shear rate measured at 215°C (Fig. 4D), showing that shear thinning started to develop at a low shear rate of ~0.1 s^{-1} and became pronounced at ~1 s^{-1}.

Summary

This work introduces a solution to three key challenges facing the development of chemically recyclable polymers: selectivity in depolymerization, trade-offs between polymers' depolymerizability and their properties and performance, and a circular monomer-polymer-monomer cycle. The results showed that, with judiciously designed monomer and polymer structures, it is possible to create chemically recyclable polymers that exhibit quantitative recyclability and useful materials properties and that the polymer synthesis and recycling processes can be performed under ambient or industrially relevant conditions.

REFERENCES AND NOTES

1. X. Zhang, M. Fevre, G. O. Jones, R. M. Waymouth, *Chem. Rev.* **118**, 839–885 (2018).
2. D. K. Schneiderman, M. A. Hillmyer, *Macromolecules* **50**, 3733–3749 (2017).
3. J. M. Garcia, M. L. Robertson, *Science* **358**, 870–872 (2017).
4. J. M. Eagan *et al*., *Science* **355**, 814–816 (2017).
5. X. Jia, C. Qin, T. Friedberger, Z. Guan, Z. Huang, *Sci. Adv.* **2**, e1501591 (2016).
6. World Economic Forum, Ellen MacArthur Foundation, and McKinsey & Company, "The new plastics economy: Rethinking the future of plastics" (Ellen MacArthur Foundation, 2016); www.ellenmacarthurfoundation.org/publications/the-new-plastics-economy-rethinking-the-future-of-plastics.
7. M. A. Hillmyer, *Science* **358**, 868–870 (2017).
8. Y. Zhu, C. Romain, C. K. Williams, *Nature* **540**, 354–362 (2016).
9. A.-C. Albertsson, M. Hakkarainen, *Science* **358**, 872–873 (2017).
10. S. Yoshida *et al*., *Science* **351**, 1196–1199 (2016).
11. N. Torres, J. J. Robin, B. Boutevin, *Eur. Polym. J.* **36**, 2075–2080 (2000).
12. M. Hong, E. Y.-X. Chen, *Green Chem.* **19**, 3692–3706 (2017).
13. A. Rahimi, J. M. García, *Nat. Rev. Chem.* **1**, 0046 (2017).
14. J. M. García *et al*., *Science* **344**, 732–735 (2014).
15. G. O. Jones, A. Yuen, R. J. Wojtecki, J. L. Hedrick, J. M. García, *Proc. Natl. Acad. Sci. U.S.A.* **113**, 7722–7726 (2016).
16. K. Fukushima *et al*., *J. Polym. Sci. A Polym. Chem.* **49**, 1273–1281 (2011).
17. J. P. MacDonald, M. P. Shaver, *Polym. Chem.* **7**, 553–559 (2016).
18. E. Lizundia, V. A. Makwana, A. Larrañaga, J. L. Vilas, M. P. Shaver, *Polym. Chem.* **8**, 3530–3538 (2017).
19. D. K. Schneiderman *et al*., *ACS Macro Lett.* **5**, 515–518 (2016).
20. Y. Liu, H. Zhou, J. Z. Guo, W. M. Ren, X. B. Lu, *Angew. Chem. Int. Ed.* **56**, 4862–4866 (2017).
21. F.-D. Kopinke, M. Remmler, K. Mackenzie, M. Möder, O. Wachsen, *Polym. Degrad. Stab.* **53**, 329–342 (1996).
22. H. Nishida *et al*., *Polym. Degrad. Stab.* **81**, 515–523 (2003).
23. C. E. Diesendruck *et al*., *Nat. Chem.* **6**, 623–628 (2014).
24. J. A. Kaitz, C. E. Diesendruck, J. S. Moore, *J. Am. Chem. Soc.* **135**, 12755–12761 (2013).
25. K. N. Houk, A. Jabbari, H. K. Hall Jr., C. Alemán, *J. Org. Chem.* **73**, 2674–2678 (2008).
26. A. Duda, A. Kowalski, in *Handbook of Ring-Opening Polymerization*, P. Dubois, O. Coulembier, J.-M. Raquez, Eds. (Wiley-VCH, 2009), chap. 1.
27. M. Hong, E. Y.-X. Chen, *Nat. Chem.* **8**, 42–49 (2016).
28. M. Hong, E. Y.-X. Chen, *Angew. Chem. Int. Ed.* **55**, 4188–4193 (2016).
29. X. Tang *et al*., *J. Am. Chem. Soc.* **138**, 14326–14337 (2016).
30. H. Haba, H. Itabashi, *Polym. J.* **46**, 89–93 (2014).
31. S. M. Anderson, B. K. Mueller, E. J. Lange, A. Senes, *J. Am. Chem. Soc.* **139**, 15774–15783 (2017).
32. J.-R. Sarasua, N. L. Rodriguez, A. L. Arraiza, E. Meaurio, *Macromolecules* **38**, 8362–8371 (2005).
33. R. Vargas, J. Garza, D. A. Dixon, B. P. Hay, *J. Am. Chem. Soc.* **122**, 4750–4755 (2000).
34. P. D. Kennewell, S. S. Matharu, J. B. Taylor, R. Westwood, P. G. Sammes, *J. Chem. Soc. Perkin Trans. 1* **0**, 2563–2570 (1982).
35. A. Amgoune, C. M. Thomas, T. Roisnel, J.-F. Carpentier, *Chemistry* **12**, 169–179 (2005).
36. A. S. Dudnik, V. L. Weidner, A. Motta, M. Delferro, T. J. Marks, *Nat. Chem.* **6**, 1100–1107 (2014).
37. J. A. Semlyen, Ed., *Cyclic Polymers* (Kluwer Academic, ed. 2, 2000).
38. K. Endo, *Adv. Polym. Sci.* **217**, 121–183 (2008).
39. H. A. Brown, R. M. Waymouth, *Acc. Chem. Res.* **46**, 2585–2596 (2013).
40. C. W. Bielawski, D. Benitez, R. H. Grubbs, *Science* **297**, 2041–2044 (2002).
41. D. A. Culkin *et al*., *Angew. Chem. Int. Ed.* **46**, 2627–2630 (2007).
42. L. Guo, D. Zhang, *J. Am. Chem. Soc.* **131**, 18072–18074 (2009).
43. J.-F. Carpentier, *Organometallics* **34**, 4175–4189 (2015).
44. A. Amgoune, C. M. Thomas, S. Ilinca, T. Roisnel, J.-F. Carpentier, *Angew. Chem. Int. Ed.* **45**, 2782–2784 (2006).
45. T. Aida, S. Inoue, *Acc. Chem. Res.* **29**, 39–48 (1996).
46. Y. Wang, W. Zhao, X. Liu, D. Cui, E. Y.-X. Chen, *Macromolecules* **45**, 6957–6965 (2012).
47. M. Cheng, A. B. Attygalle, E. B. Lobkovsky, G. W. Coates, *J. Am. Chem. Soc.* **121**, 11583–11584 (1999).
48. J. M. Longo, A. M. DiCiccio, G. W. Coates, *J. Am. Chem. Soc.* **136**, 15897–15900 (2014).
49. J. Slager, A. J. Domb, *Adv. Drug Delivery Rev.* **55**, 549–583 (2003).
50. J. Kumaki, T. Kawauchi, K. Okoshi, H. Kusanagi, E. Yashima, *Angew. Chem. Int. Ed.* **46**, 5348–5351 (2007).
51. K. Fukushima, Y. Kimura, *Polym. Int.* **55**, 626–642 (2006).
52. A. M. Liquori, *et al*., *Nature* **206**, 358–362 (1965).
53. I. Engelberg, J. Kohn, *Biomaterials* **12**, 292–304 (1991).

ACKNOWLEDGMENTS

We thank B. Boyle for assistance with rheology studies, as well as H. Sardon and A. Sangroniz for discussions. **Funding:** This work was supported by the NSF (grant NSF-1664915) and the W. M. Keck Foundation. **Author contributions:** E.Y.-X.C. conceived the project and directed research. J.-B.Z. designed and conducted experiments related to monomer and polymer synthesis. J.-B.Z., E.M.W., and J.T. designed and conducted experiments related to polymer characterizations. J.-B.Z. and E.Y.-X.C. wrote the initial manuscript, and all authors contributed to the revised manuscript. **Competing interests:** E.Y.-X. C. and J.-B.Z. are inventors on U.S. patent application 62/540,672, submitted by Colorado State University Research Foundation, which covers the herein-described recyclable polymer system and its stereocomplexes. E.M.W. and J.T. declare no competing interests. **Data and materials availability:** All data needed to evaluate the conclusions in the paper are present in the paper and/or the supplementary materials.

SUPPLEMENTARY MATERIALS

www.sciencemag.org/content/360/6387/398/suppl/DC1
Materials and Methods
Supplementary Text
Figs. S1 to S87
Tables S1 to S3
References (*54*–*56*)

21 November 2017; accepted 9 March 2018
10.1126/science.aar5498